Power System Stability Control for a Wind Farm Based on Adaptive Dynamic Programming

Yufei Tang, *Student Member, IEEE*, Haibo He, *Senior Member, IEEE*, Jinyu Wen, *Member, IEEE*, and Ju Liu, *Student Member, IEEE*

***Abstract*—In this paper, a goal representation heuristic dynamic programming (GrHDP) based controller is developed for the doubly-fed induction generator based wind farm to improve the system transient stability under fault conditions. The proposed controller is based on adaptive dynamic programming (ADP) techniques to approximate the optimal control policy according to the interaction between the controller and the power plant. Compared to existing ADP approaches with one action network and one critic network, our GrHDP architecture introduces an additional network, i.e., the reference network, to form an internal goal/reward representation. This better mapping between the system state and the control action significantly improves the control performance. The effectiveness of the proposed approach is validated via two cases. The first case investigates a revised four-machine two-area system with high wind penetration and a static synchronous compensator. The second case is a practical size power system with wind farm in Liaoning Province in China. Detailed simulation analysis and comparative studies with traditional ADP approaches are presented to demonstrate the superior performance of our method.**

***Index Terms*—Computational intelligence (CI), doubly-fed induction generator (DFIG), goal representation heuristic dynamic programming (GrHDP), power system stability.**

I. Introduction

THE INCREASING wind generation with long-distance power transmission in electrical power grids raise reasonable concern of possible stability threats to the system security operation and control. In such situations, how to design an adaptive, optimal controller becomes a critical challenge faced by the power grid operators and engineers around the world today. Among many enabling technologies, the latest research results from both the power and energy community and the computational intelligence (CI) community have demonstrated that CI research could provide key technical innovations to solve this challenging problem. Thereby in this paper, a goal representation heuristic dynamic programming (GrHDP) based approach is adopted to improve the transient stability of power systems with wind penetration under fault conditions.

Doubly-fed induction generators (DFIGs) are the most widely used wind power generators in wind power generation systems [1]. It has been recognized that the controllers have a critical impact on the stability performance of grid-connected DFIG. Therefore, the controllers should be designed appropriately [2]. Among all the control designs, reactive power control is an important issue for the grid-connected wind farms [3]–[5]. Many wind power grid connection codes today require the enhancement of the low voltage ride-through (LVRT) capability of wind farms and the maintenance of their reliability in a certain range during and after a short-term fault. The study in [3] shows that rotor angles of synchronous generators are directly influenced by the type of reactive power control employed by the wind generation. The implementation of appropriate control strategies in wind farms, particularly the terminal voltage control, can lessen the reactive power requirements of conventional synchronous units and help to mitigate large rotor angle swings. Meanwhile, it is suggested that a good control strategy for the static synchronous compensator (STATCOM) will significantly improve the system dynamics [6], [7]. Based on this suggestion, an approach to conduct an impact study of a STATCOM on the integration of a large wind farm into a weak loop power system is presented in [8]. Here it is illustrated that the size and location of the STATCOM will both affect the voltage fluctuations.

A decoupled control technique for the active and reactive power of doubly-fed wound rotor induction generator is proposed in [9], and it has been widely used in the control design of wind turbines (WT) with DFIG [10]–[12]. The control technique is based on the conventional proportional-integral (PI) control, which needs an accurate wind farm and power system model. Therefore, this technique requires a large number of parameters to be optimized or tuned to ensure a good interaction between the wind farm and the power system at the point of common coupling (PCC). For most of the research, the parameters of the PI controllers are tuned with approximate linearization using different optimization methods. For instance, Wu *et al.* [11] present an approach to use particle swarm optimization (PSO) to optimize the control parameters in a DFIG simultaneously based on a system-level fitness function. However, when the number of the DFIG in the system

Manuscript received May 14, 2013; revised November 27, 2013, February 27, 2014, and June 2, 2014; accepted July 12, 2014. This work was supported in part by the National Science Foundation (NSF) under Grant ECCS 1053717, in part by the Army Research Office under Grant W911NF-12-1-0378, in part by the NSF-Deutsche Forschungsgemeinschaft Collaborative Research on Autonomous Learning under Supplement Grant CNS 1117314, and in part by the National Natural Science Foundation of China under Grant 51228701. Paper no. TSG-00382-2013.

Y. Tang and H. He are with the Department of Electrical, Computer, and Biomedical Engineering, University of Rhode Island, Kingston, RI 02881 USA (e-mail: ytang@ele.uri.edu; he@ele.uri.edu).

J. Wen and J. Liu are with the College of Electrical, Electronic, and Engineering, Huazhong University of Science and Technology, Wuhan 430074, China (e-mail: jinyu.wen@hust.edu.cn; liujhust@smail.hust.edu.cn).

Color versions of one or more of the figures in this paper are available online at http://ieeexplore.ieee.org.

Digital Object Identifier 10.1109/TSG.2014.2346740

increases, the number of control parameters will also increase significantly leading to the curse of dimensionality issue.

Intelligent control strategies, such as fuzzy logic, has been successfully applied to control DFIG in different applications [13]–[15]. In [13], neuro-fuzzy vector control is implemented on a laboratory DFIG. In [14], fuzzy logic control is used for primary frequency and active power control of the wind farms. In [15], a methodology to design an adaptive maximum power point tracking fuzzy system for variable speed wind generators is proposed and tested. Such fuzzy system has low memory occupancy and high learning capability, overcoming some disadvantages of classical sensor-less peak power tracking control methods, thus could be well implemented on a micro-controller. However, all these aforementioned fuzzy controls require sufficient off-line fine tuning and simulation, which limit their large-scale applications.

After more than twenty years of studies in intelligent control in power systems, advanced control approaches, such as adaptive dynamic programming (ADP) based methods, have shown to be promising for power system control problems [16]–[20]. Qiao *et al.* [18] propose a heuristic dynamic programming (HDP) based coordinated reactive power control of a large wind farm and a STATCOM. The HDP based controller shows improved performance of the DFIG in presence of a grid fault, with the assumption that the controller has been sufficiently pretrained based on the information from the environment before connected to the grid. Meanwhile, another category of "model free" ADP approach [21], which does not require a detailed model of the environment or model network to predict the system status, has successfully demonstrated its effectiveness in many real applications including damping control in a classic four-machine two-area system and a real large power system in China [22], among others [23]–[26]. The classical HDP approach has been demonstrated to be a feasible technique to damp oscillation and to increase power system stability. However, the reinforcement signal in the classical HDP has been designed in a "hand-crafted" way, which may not adapt with the system operating conditions. For instance, many of the classic HDP methods simply use a binary reinforcement signal, such as a "+1" and a "−1" to represent the "success" or "failure" of the control. Inspired by our previous work in [27] and [28], in this paper, we develop the wind farm power system stability control based on the new GrHDP. By introducing of a new reference network to provide an internal goal signal to the critic network, our GrHDP architecture forms an internal goal/reward representation that can provide a rich representation of the control objective compared to the traditional design. In this paper, we aim to investigate the reactive power control of a wind farm to improve the system dynamics during and after grid fault, namely, to reduce the oscillation overshoot and increase the damping of the system.

The rest of the paper is organized as follows. Section II presents the revised four-machine two-area system and the detailed model of each part, including the DFIG model, DFIG controller and STATCOM controller model. Section III presents the GrHDP structure and the design of the power system controller. Section IV presents simulation results of the first of two cases in MATLAB/Simulink environment with two

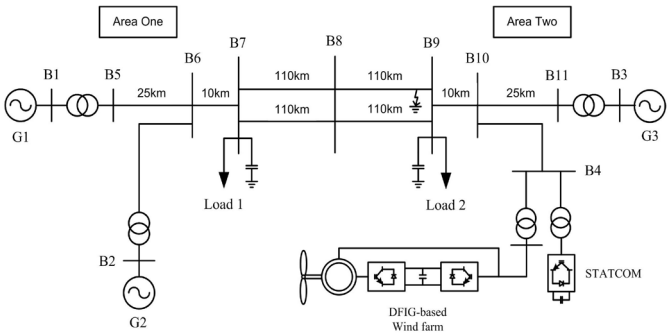

Fig. 1. Single-line diagram of the benchmark power system that includes a DFIG-based wind farm and a STATCOM.

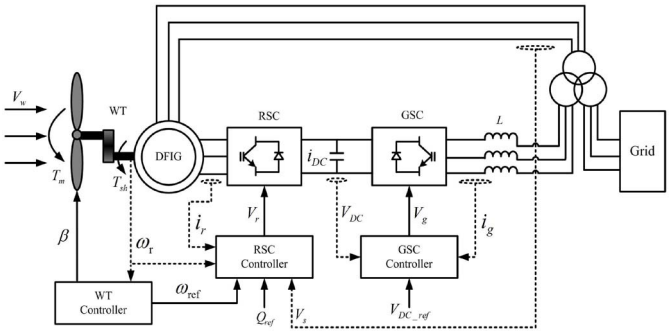

Fig. 2. Schematic diagram of DFIG wind turbine system [4], [5].

different scenarios. Section V demonstrates the control performance in another case with an equivalent practical size wind farm system. Section VI concludes the paper and addresses some implementation considerations.

II. System Configuration and Modeling

A. Overview Power System Configuration

Fig. 1 shows the revised four-machine two-area system, which is based on the classic model. This benchmark power system has been first investigated in [10] to study the wind turbine with different controllers, such as the optimized PI controller or the nonlinear controller, to improve the transient stability performance of the power system. The system is divided into two areas, in each of which there are two machines. In [10], the four-machine two-area system is modified by replacing generator 3 (G3) with a DFIG-based wind farm. In this paper, instead of replacing G3 with a wind farm, the generator 4 (G4) is replaced with a DFIG-based wind farm and a STATCOM. The parameters of the benchmark system and the power flow can be referenced in [10].

B. DFIG Wind Turbine System Model

Fig. 2 illustrates the wind turbine model studied in this paper [4], [5]. In this system, the WT is connected to the DFIG through a drive train system, which consists of a low and a high speed shaft with a gearbox in between. The WT with DFIG system is an induction type generator in which the stator windings are directly connected to the three-phase grid, and the rotor windings are fed through three-phase back-to-back insulated-gate bipolar transistor (IGBT) based

pulse width modulation (PWM) converters. The back-to-back PWM converter consists of a rotor-side converter (RSC), a grid-side converter (GSC) and a dc-link capacitor. Their controllers include three parts: a RSC controller, a GSC controller, and a wind turbine controller. Generally speaking, the objectives of these controllers are to maximize power production while maintaining the desired rotor speed and voltage [5]. Specifically, the WT controller controls the pitch angle of the wind turbine and the reference rotor speed to the RSC and GSC controller. Two control mechanisms are used: 1) power optimization mechanism with sub-synchronous speed; and 2) power limitation mechanism with super-synchronous speed. The RSC and GSC controller are to control the active and reactive power of the DFIG using vector control technique.

1) Model of Drive Train: The drive train system consists of a turbine, a low and a high speed shaft, and a gearbox. This system can be represented by a two-mass model as follows [11]:

$$2H_t\frac{d\omega}{dt} = T_m - T_{sh} \tag{1}$$

$$\frac{d\theta_{tw}}{dt} = \omega_t - \omega_r = \omega_t - (1-s_r)\omega_s \tag{2}$$

$$2H_g\frac{ds_r}{dt} = -T_{em} - T_{sh} \tag{3}$$

$$T_{sh} = K_{sh}\theta_{tw} + D_{sh}\frac{d\theta_{tw}}{dt} \tag{4}$$

where

H_t	the inertia constants of the turbine;
H_g	the inertia constants of the generator;
ω_t	the WT angle speed;
ω_r	the generator rotor angle speed;
$\theta_{t\omega}$	the shaft twist angle;
K_{sh}	the shaft stiffness coefficient;
D_{sh}	the damping coefficient;
T_{sh}	the shaft torque;
T_m	the wind torque;
T_{em}	the electromagnetic torque.

2) Model of Rotor Side Controller: The RSC controller aims to control the DFIG output active power for tracking the input of the WT torque, and to maintain the terminal voltage in control setting [11]. As we mentioned before, the vector control strategy is used for the active power and reactive power control of the WT with DFIG system. In order to decouple the electromagnetic torque and the rotor excitation current, the induction generator is controlled in the stator-flux-oriented reference frame, which is synchronously rotating, with its d axis oriented along the stator-flux vector position [2], [4]. Thus, for the RSC, the active power and voltage are controlled independently via v_{qr} and v_{dr}, respectively. The voltage control is achieved by controlling the reactive power to keep it within the desired range. Fig. 3 is the overall vector control scheme of the RSC. The rotor speed w_r and Q_s are the measured system active power and reactive power, respectively. They are compared with the desired active power and reactive power to generate the reference signals i_{qr_ref} and i_{dr_ref}. The actual $d-q$ current signals i_{qr} and i_{dr} are then compared with these reference signals to generate the error signals, which are passed through two PI controllers to form the voltage signal references v^*_{qr} and v^*_{dr}, respectively. The two voltage signals v^*_{qr} and v^*_{dr} are compensated by the corresponding cross-coupling terms to form the voltage signals v_{qr} and v_{dr}. After reference frame transformation, control signal V_r is then used by the PWM module to generate the IGBT gate control signals to drive the RSC.

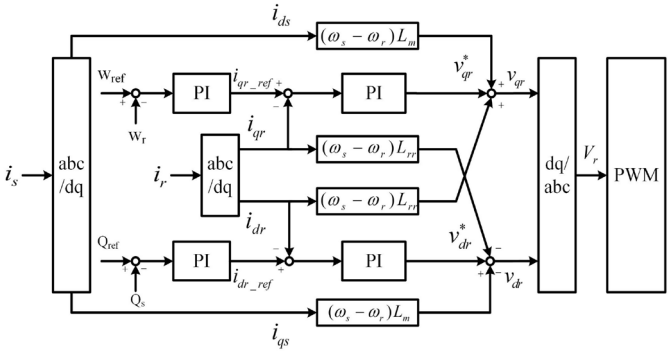

Fig. 3. Schematic diagram of rotor side controller.

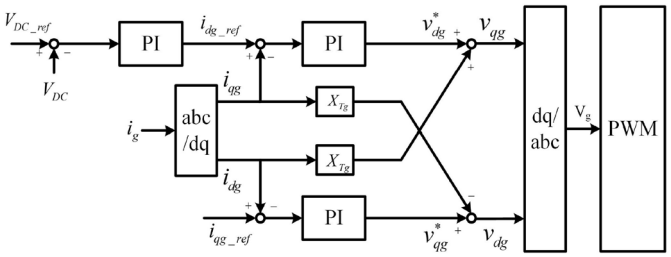

Fig. 4. Schematic diagram of grid side controller.

3) Model of Grid Side Controller: The GSC, as showed in Fig. 4, aims to maintain the dc-link voltage, and to control the terminal reactive power [11]. In order to obtain independent control of the active and reactive power flowing between the grid and the grid side converter, the converter control operates in the grid-voltage oriented reference frame, which is synchronously rotating, with its d axis oriented along the grid-voltage vector position [2], [4]. Thus, the dc-link voltage and reactive power are controlled independently via v_{dg} and v_{qg}, respectively. The actual signal of the dc-link voltage V_{DC} is compared with its command value V_{DC_ref} to form the error signal, which is passed through the PI controller to generate the reference signal i_{dg_ref}. Then this reference signal i_{dg_ref} and another corresponding reference signal i_{qg_ref} are compared with the actual signals i_{qg} and i_{dg}, respectively. These error signals are then passed through two PI controllers to form the voltage signal references v^*_{dg} and v^*_{qg}, respectively. The two voltage signals v^*_{dg} and v^*_{qg} are compensated by the corresponding cross-coupling terms to form the voltage signals v_{dg} and v_{qg}. After reference frame transformation, control signal V_g is then used by the PWM module to generate the IGBT gate control signals to drive the GSC.

C. STATCOM Model

The STATCOM and its controllers are shown in Fig. 5. It is a shunt device of the flexible alternating current transmission system (FACTS) family using power electronics to

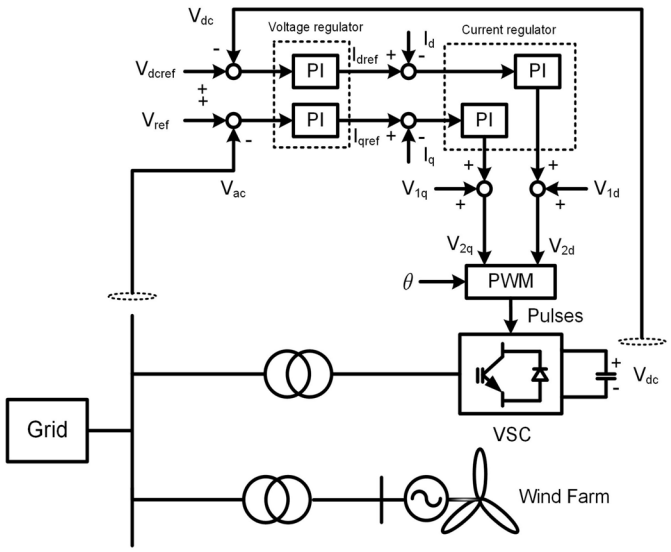

Fig. 5. Schematic diagram of STATCOM control.

control power flow and improve transient stability of power grids [6]–[8]. The STATCOM regulates voltage at its terminal by controlling the amount reactive power injected into or absorbed from the power grid, which depends on the system voltage. The STATCOM modeling is based on IGBT, but as details of the inverter and harmonics are not represented, it can also be used to model a gate-turn-off thyristor (GTO) based STATCOM in transient stability studies. In the controller design, an outer regulation loop consists of an ac voltage regulator and a dc voltage regulator, while an inner regulation loop consists of a current regulator. The current regulator is assisted by a feed forward type regulator which predicts V_{2d} and V_{2q} from the measurements V_{1d}, V_{1q} and the transformer leakage reactance [6].

During normal conditions, both active and reactive power flow to/from the STATCOM are very low. Active power demand is only the losses within the STATCOM, and reactive power demand is within the difference between neighbor steps of switchable ac filters [29]. When the system is under fault conditions, both STATCOM active and reactive power demands are significantly increased. Because of the high cost, the rating of the STATCOM should be carefully addressed in practical applications. The minimal capacity of STATCOM should be chosen above the given curve for particular value of communication delay. A detailed engineering study of the STATCOM sizing is presented in [29]. In this paper, the parameters of the STATCOM in the simulation are given in the Appendix.

III. GrHDP-Based Controller Design

The GrHDP architecture includes three parts: an action network, a critic network, and a reference network [27], [28]. The action network produces control signal $u(t)$ according to a learning policy represented by approximating network, while the reference network provides the internal reinforcement signal (internal goal/reward representation) $s(t)$, to interact with the critic network to approximate the cost and reward function J by minimizing the Bellman function as follows:

$$J^*(x(t)) = \min_{u(t)} \left\{ U(x(t), u(t)) + \gamma * J^*(x(t+1)) \right\} \tag{5}$$

where $x(t)$ is the state vector of the system, U is the utility function, and γ is a discount factor. These three parts are usually implemented by using neural networks because of their universal approximation capability and the associated back-propagation learning algorithm. During the on-line learning, the controller is "naive" when it starts to control, namely, the action network, critic network and reference network are both randomly initialized in their weights. Once a system state is observed, an action will be subsequently produced based on the parameters in the action network. The principle in adapting the action network is to indirectly back propagate the error between the desired ultimate objective, denoted by U_c, and the approximate J function from the critic network. Based on the instant reinforcement signal and internal reinforcement signal, the controller will learn to accomplish the control goal. The error functions used to update the parameters in the action network, critic network and reference network are as follows:

$$\begin{cases} e_a(t) = J(t) - U_c(t); & E_a(t) = \frac{1}{2} e_a^2(t) \\ e_f(t) = \alpha J(t) - [J(t-1) - r(t)]; & E_f(t) = \frac{1}{2} e_f^2(t) \\ e_c(t) = \alpha J(t) - [J(t-1) - s(t)]; & E_c(t) = \frac{1}{2} e_c^2(t). \end{cases} \tag{6}$$

The chain back-propagation rule is employed to train and adapt the parameters in the three neural networks as follows:

$$\begin{cases} \frac{\partial E_a(t)}{\partial \omega_a(t)} = \frac{\partial E_a(t)}{\partial J(t)} \frac{\partial J(t)}{\partial u(t)} \frac{\partial u(t)}{\partial \omega_a(t)} \\ \frac{\partial E_f(t)}{\partial \omega_f(t)} = \frac{\partial E_f(t)}{\partial J(t)} \frac{\partial J(t)}{\partial s(t)} \frac{\partial s(t)}{\partial \omega_f(t)} \\ \frac{\partial E_c(t)}{\partial \omega_c(t)} = \frac{\partial E_c(t)}{\partial J(t)} \frac{\partial J(t)}{\partial \omega_c(t)} \end{cases} \tag{7}$$

where ω_a, ω_f and ω_c are the weights of action network, reference network and critic network, respectively.

Fig. 6 shows the DFIG wind turbine system and STATCOM with the proposed GrHDP controller. The upper area denotes the plant to be controlled by the GrHDP controller. The system state $X(t)$ is measured as the GrHDP controller input signal. Then the output signal or action signal $u(t)$ is produced by the controller as supplementary control signals send to the RSC controller and the STATCOM controller, plus the steady state values to form the total command signals. The detailed design of the controller including the input, output and reinforcement signal will be illustrated in the following section.

A. Input, Output, and Reinforcement Signal Design

As an on-line controller with instant learning from the environment, the performance of the GrHDP controller is mainly depend on the design of the input, output and reinforcement signal. Figs. 7 and 8 show active power from area one to area two and active power of the wind farm after a three-phase ground-fault applied at 5 s, respectively. The applied fault causes oscillation of the active power of the whole system. After the fault, the active power of the wind farm (Fig. 8)

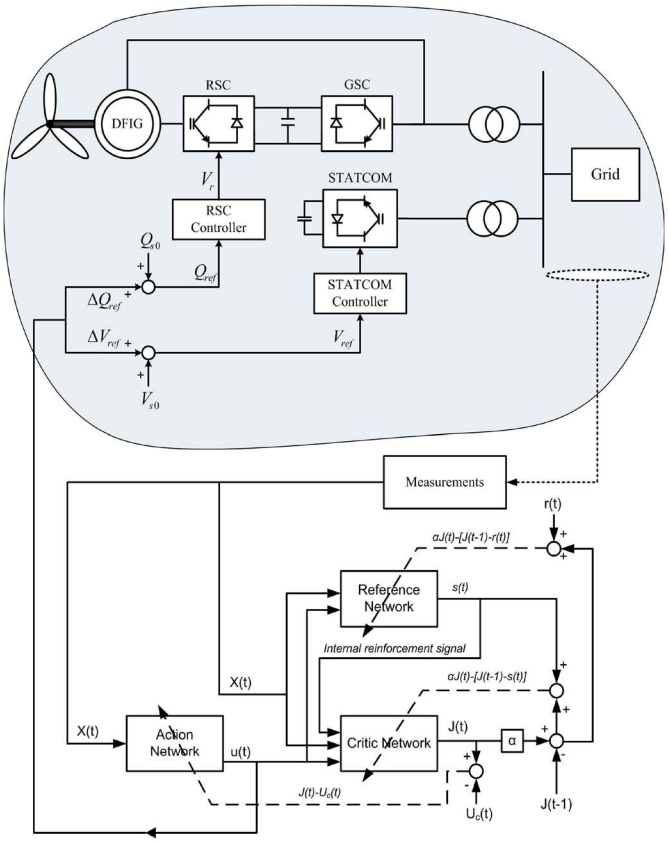

Fig. 6. Schematic diagram of the GrHDP controller with the plant.

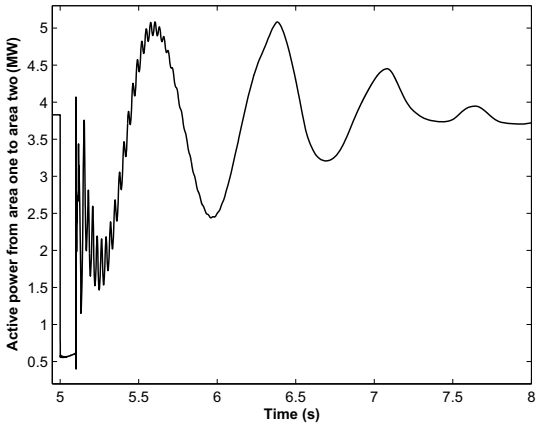

Fig. 7. Active power from area one to area two after system fault.

damps within about 1 s, but the transferred active power oscillation (Fig. 7) lasts much longer, i.e., 3 s. So it is reasonable to consider the system dynamics (oscillation between the two areas) into the input, output and reinforcement signal design. The input signal of the controller is designed as follows:

$$\begin{cases} \Delta V_{\text{wind}}(t),\ \Delta V_{\text{wind}}(t-1),\ \Delta V_{\text{wind}}(t-2) \\ \Delta P_{\text{wind}}(t),\ \Delta P_{\text{wind}}(t-1),\ \Delta P_{\text{wind}}(t-2) \\ \Delta P_{12}(t),\quad \Delta P_{12}(t-1),\quad \Delta P_{12}(t-2) \end{cases} \tag{8}$$

where ΔV_{wind} is the voltage deviation of the wind farm, ΔP_{wind} is the active power deviation of the wind farm

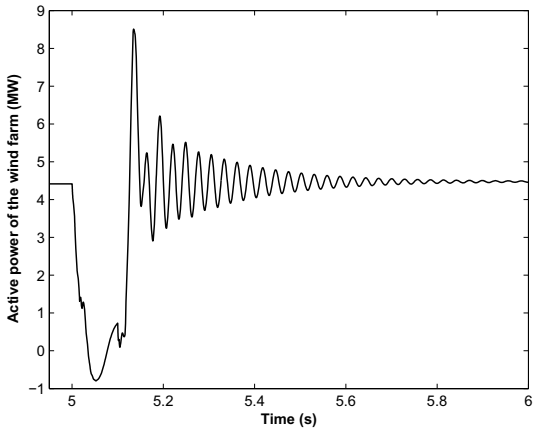

Fig. 8. Active power of the wind farm after system fault.

and ΔP_{12} is the deviation of transferred active power from area one to area two. The output signals of the controller are $\Delta Q_{\text{ref}}(t)$ and $\Delta V_{\text{ref}}(t)$, which are send to the wind farm and the STATCOM as supplementary control signals. The reinforcement signal of the controller is designed as follows:

$$\begin{aligned} r(t) = &-\Delta V^2_{\text{wind}}(t) - 0.5 * \Delta V^2_{\text{wind}}(t-1) \\ &-0.1 * \Delta V^2_{\text{wind}}(t-2) - \Delta P^2_{\text{wind}}(t) \\ &-0.5 * \Delta P^2_{\text{wind}}(t-1) - 0.1 * \Delta P^2_{\text{wind}}(t-2) \\ &-\Delta P^2_{12}(t) - 0.5 * \Delta P^2_{12}(t-1) - 0.1 * \Delta P^2_{12}(t-2) \\ &-3 * \Delta \omega^2_{12}(t) \end{aligned} \tag{9}$$

where Δw_{12} is the oscillation between the two areas. In this paper, we choose the rotor angle difference between G1 and G3 to represent area oscillation.

The principle of the GrHDP controller for the benchmark power system is discussed as follows. When the system is under fault conditions, the supplementary control signals ΔV_{ref} and ΔQ_{ref} will change with the system states. With appropriate adjustment, the controller can reduce the level of voltage dips of the wind farm as well as the PCC point, and improve the transient stability of the whole system after the fault. Because of the direct coupling between the voltage and the reactive power, it is straightforward to use the voltage deviation ΔV_{wind} as the first of the three input signals to the controller. The active power deviation of the wind farm ΔP_{wind} is also considered as the second input signal to the GrHDP controller to provide additional information, thus providing better control performance [18]. As we mentioned before, since the dynamics of the system last longer than (that of) the wind farm, therefore the deviation of the transferred active power from area one to area two (i.e., ΔP_{12}) is also considered as the third and last input signal. The design of the reinforcement signal $r(t)$ in (9) is based on the external environment, which is represented by the wind farm and the system oscillation. The control of the wind farm and the STATCOM is coordinated, to some extent, as the system states are combined in one index as indicated in the designed $r(t)$.

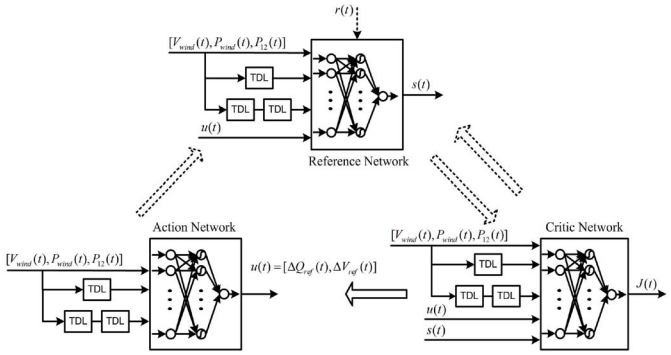

Fig. 9. Implementation and cooperative learning of the GrHDP controller.

B. Implementation of the Action, Critic, and Reference Network

Fig. 9 shows the implementation of the action, critic, and reference network. We can observe that, the $s(t)$ signal provides an important link between the reference network and the critic network, which makes the chain back-propagation able to adjust the parameters in the reference network and critic network. Furthermore, compared with the classical ADP, the $s(t)$ signal is served as an adaptive reinforcement signal $r(t)$ to the critical network. In this way, multiple-level internal goals are formed by the GrHDP to fulfill the long-term final goal. A cooperative learning strategy is used which involves more interactions between the reference network and the critic network [27]. In this learning strategy, at each epoch of the parameter tuning, one can first adapt the reference network weights based on the primary reinforcement signal $r(t)$ through back-propagation. Then the reference network will output the secondary reinforcement signal $s(t)$, which will be used to tune the weights in the critic network through back-propagation. Once the weights in critic network are tuned in this epoch, the critic network will provide a new $J(t)$ estimation, which in turn can be used to adapt the weights in reference network in the next epoch. In this way, the reference network and critic network are trained in a more collaborative style.

The controller work flow is summarized as follows.

1) The action network receives the measured plant state deviations $\Delta P_{\text{wind}}(t)$, $\Delta Q_{\text{wind}}(t)$, and $\Delta P_{12}(t)$, then these signals are used to generate temporary control signals $\Delta Q'_{\text{ref}}(t)$ and $\Delta V'_{\text{ref}}(t)$.
2) The reference network will update its weights according to (7) first. Then the external reinforcement signal $r(t)$, plant state deviations $\Delta P_{\text{wind}}(t)$, $\Delta Q_{\text{wind}}(t)$, $\Delta P_{12}(t)$, and temporary control signals $\Delta Q'_{\text{ref}}(t)$ and $\Delta V'_{\text{ref}}(t)$ are used to generate the internal reinforcement signal $s(t)$.
3) The critic network will update its weights according to (7) using above internal reinforcement signal $s(t)$. Then the internal reinforcement signal $s(t)$, plant state deviations $\Delta P_{\text{wind}}(t)$, $\Delta Q_{\text{wind}}(t)$, $\Delta P_{12}(t)$, and temporary control signals $\Delta Q'_{\text{ref}}(t)$ and $\Delta V'_{\text{ref}}(t)$ are used to estimate the cost function J.
4) Because of the adopted cooperative learning strategy, above two steps are performed alternately until the stop criterion is satisfied.
5) Having finished the adaptation in the reference network and critic network, the action network will update its weights according to (7) until the stop criterion is satisfied. Then the final control signals $\Delta Q_{\text{ref}}(t)$ and $\Delta V_{\text{ref}}(t)$ are generated and send to the wind farm and the STATCOM.
6) Above steps are repeated at each simulation time step until the end of the simulation.

C. Remarks of GrHDP Controller for Power System

The reinforcement learning based GrHDP controller is a supplement to the traditional controllers, such as power system stabilizer (PSS) and PI controller in DFIG. PSS is primarily used to damp low frequency oscillations in the range of 0.2 to 2.5 Hz. These oscillations result from the rotors of synchronous machines oscillate with each other using transmission lines between them to exchange energy [30]. The problem is exacerbated as wind farms are always located in remote areas where long-distance transmission lines are required. The DFIG based wind generation with PSS is first introduced in [31]. The PSS is specific designed on the DFIG with a flux magnitude angle controller (FMAC), where this form of PSS control could be applied to other DFIG control schemes with appropriate modifications [32], [33]. However, most of the PSS and PI controller designs in DFIG are based on linear control theory which require a nominal power system model formulated as a linear, time-invariant system. And the nominal design model is obtained for a particular operating condition. After off-line tuning of the parameters, extensive field testing is required to test the effectiveness of the controller. The designed controller based on this approach can be very well tuned to an operating condition and will provide good damping over a certain range around the design point. However, power systems are nonlinear systems with wide range of operating conditions and time-varying configurations. Also, it has been found that the dynamic properties of the power systems are quite different for different operating conditions. This situation is much more severe for the variations of wind speed and DFIG operating mode [34]. Therefore, the fixed parameters of the traditional controllers may not be optimal for the whole set of possible operating conditions and configurations.

The traditional controller designs are based on linear analysis tools such as eigenvalue analysis, bode diagram, Nyquist diagram, etc. [30]. In contrast, the GrHDP is based on on-line learning to adjust its parameters to minimize the reinforcement signal. Because of the universal approximation capability of the neural network, it is possible to find the right mapping between the input and output signal to damp the system oscillation. As common sense, the initial weights are quite important for the performance of the on-line learning GrHDP. Trial-and-error approach is used in this paper, and a typical learning process includes two trials [22], [26], [35]. In trial one, since the randomly initialization, the mapping between the input (ΔV_{wind}, ΔP_{wind}, ΔP_{12}) and output $u(t)$ is not in accordance with expectation, thus the system dynamics may not be improved. However, trial one provides the GrHDP controller

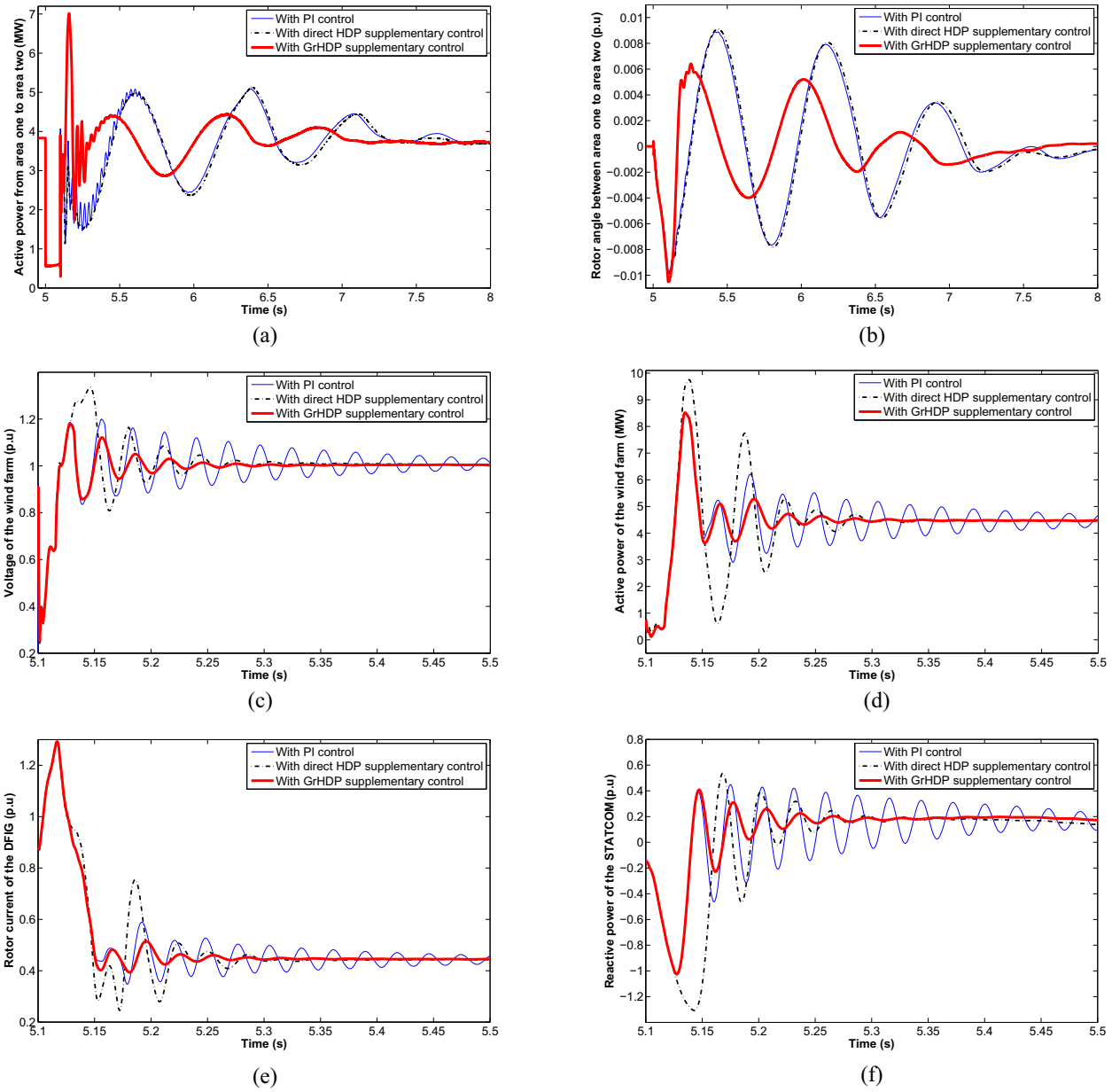

Fig. 10. Dynamics of the benchmark power system in Case One under Scenario I. (a) Active power from area one to area two. (b) Rotor angle between area one and area two. (c) Voltage of the wind farm. (d) Active power of the wind farm. (e) Rotor current of the DFIG. (f) Reactive power of the STATCOM.

useful information about which input∼output pairs may not effect and should therefore be avoided. Then in trial two, instead of random initialization, the weights in trial one is carried on and the expected input∼output pairs can be achieved.

IV. Simulation Results of Case One

The proposed GrHDP controller and the benchmark power system is implemented in MATLAB/Simulink environment. To make comprehensive comparison, the traditional ADP (i.e., direct HDP) algorithm in [21] is also applied to control the DFIG-based wind farm and the STATCOM. Simulations are performed on the benchmark power system in Fig. 1 under two scenarios to verify the effectiveness of the proposed controller. During the simulation, all the synchronous machines are equipped with automatic voltage regulator (AVR), speed regulator, and PSS. The proposed GrHDP controller provides supplementary control signals to the regular PI controllers in DFIG and STATCOM.

A. Scenario I

In this scenario, the wind speed is kept constant at 11 m/s. The steady state commands of DFIG and STATCOM are set as $Q_{s0} = 0$ and $V_{s0} = 1$, respectively. A three-phase ground-fault with ground resistance of 0.01Ω is applied at B9 at $t = 5$ s, where the fault is cleared at $t = 5.1$ s without tripping the line. The simulations are carried out to compare the transient dynamics of the wind farm and the system using the GrHDP controller, direct HDP controller and PI controller.

Fig. 10 demonstrates the simulation results of various variables of this benchmark under the situation of with GrHDP

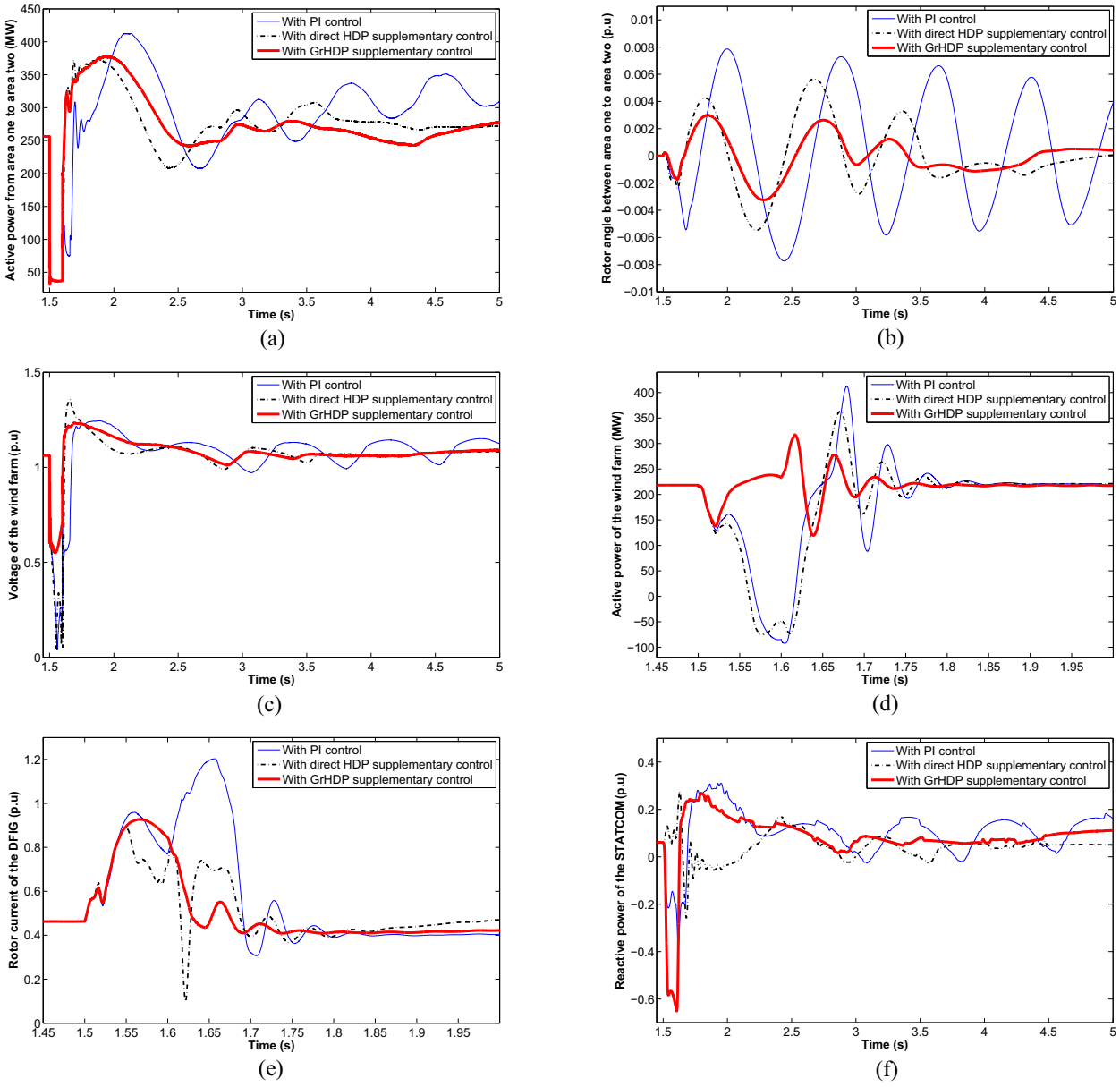

Fig. 11. Dynamics of the benchmark power system in Case One under Scenario II. (a) Active power from area one to area two. (b) Rotor angle between area one and area two. (c) Voltage of the wind farm. (d) Active power of the wind farm. (e) Rotor current of the DFIG. (f) Reactive power of the STATCOM.

controller, direct HDP controller and PI controller. Specifically, Fig. 10(a) shows the transferred active power from area one to area two, Fig. 10(b) shows the rotor angle difference between the two areas, Fig. 10(c) shows the voltage of the wind farm, Fig. 10(d) shows the active power of the wind farm, Fig. 10(e) shows the DFIG rotor current, and Fig. 10(f) shows the reactive power of the STATCOM. It can be observed that by applying the GrHDP controller and direct HDP controller, the transient stability of the wind farm and system has been improved and the oscillations of the system and the wind farm have been damped quickly after the fault. Moreover, the control effect of the proposed GrHDP controller is much better than the direct HDP controller. The oscillation of the transferred active power from area one to area two and rotor angle difference between the two areas are much smaller with the proposed GrHDP controller.

B. Scenario II

To verify the robustness of the proposed GrHDP controller, the configuration of the benchmark power system in Fig. 1 is modified. Specifically, the capacity of G1, G2, G3, and G4 are increased from 9 to 400 MW. Meanwhile, we assume one of the transmission lines between these two areas (the lower one in Fig. 1) is out-of-service, which represents the system is much more vulnerable than the original one. The speed of the wind in the DFIG-based wind farm is kept constant at 11 m/s. The steady state commands of DFIG and STATCOM are the same as before with $Q_{s0} = 0$ and $V_{s0} = 1$, respectively. A three-phase ground-fault with ground resistance of 0.01Ω is applied near B8 at $t = 1.5$ s, and the fault is cleared at $t = 1.6$ s without tripping the line.

Fig. 11 demonstrates the simulation results of various variables of this benchmark under the situation of with GrHDP controller, direct HDP controller and PI controller. Specifically,

Fig. 12. Geography information of the Liaoning Zhangdong wind farm.

Fig. 11(a) shows the transferred active power from area one to area two, Fig. 11(b) shows the rotor angle difference between the two areas, Fig. 11(c) shows the voltage of the wind farm, Fig. 11(d) shows the active power of the wind farm, Fig. 11(e) shows the DFIG rotor current, and Fig. 11(f) shows the reactive of the STATCOM. These results still demonstrate that the system is stable while applying the GrHDP controller and the direct HDP controller, and the transient dynamics of the wind farm and the system have been improved. With the GrHDP controller, the LVRT capability of the wind farm has been improved significantly compared with the other two methods. Moreover, these results indicate the robust optimization capability of the proposed GrHDP controller: when the system operation condition or configuration changes, the GrHDP controller still demonstrates satisfied control performance.

V. Practical Size Power System Control Case

Zhangdong wind farm is located in Zhangwu county in the northwestern part of Liaoning Province in China. Since the abundant wind energy source, the total installed wind power capacity in this area has reached 700 MW in the year of 2012. The geography information of the wind farm is shown in Fig. 12, where the equivalent Zhangdong wind farm system is shown in Fig. 13. We can see that the wind farm output power are first collected at Zhangwu 35 kV bus, then stepped up by transformer to 220 kV transmission lines, and finally connected to the main grid of Liaoning Province through 500 kV bus. The equivalent wind farm system is modeled in MATLAB/Simulink environment in this paper. The network power flow data and geometry information of a typical winter day in 2012 is adopted. The bus parameters of Zhangdong wind farm system are shown in Table I. In this table, 1 represents slack bus, 2 represents PV bus, and 3 represents PQ bus. P_g and Q_g are the generated active power and reactive power, respectively. P_l and Q_l are the active load and reactive load, respectively. All the values are under the base of 100 MVA. The frequency of the system is $f = 50$ Hz.

The transmission line parameters of Zhangdong wind farm system are shown in Table II.

TABLE I
Zhangdong Wind Farm System Data: Bus

Bus No.	Type	P_g	Q_g	P_l	Q_l	Voltage (kV)
1	2	6	0.91	0	0	20
2	3	0	0	0	0	220
3	3	0	0	0.7	0.15	220
4	3	0	0	1.18	0.249	220
5	3	0	0	0	0	220
6	3	0	0	0	0	220
7	3	0	0	0	0	220
8	1	0	0	0	0	500
9	3	-6.11	3.03	0	0	500
10	3	0	0	1.958	0.106	220
11	3	0	0	3	1	220
12	3	0	0	0	0	220
13	3	0	0	1.56	0.25	220
14	3	0	0	0.53	0.078	220
15	2	3.46	0	0	0	35
16	2	6	2.38	0	0	20

TABLE II
Zhangdong Wind Farm System Data: Transmission Line

From	To	Resistance	Reactance	Susceptance	Ratio
1	2	0.0004	0.02355	0	1
2	3	0.001131	0.010327	0.03263	0
2	3	0.00134	0.010137	0.032934	0
3	4	0.002467	0.012564	0.036174	0
3	4	0.0024	0.0141	0.0394	0
4	5	0.003785	0.035893	0.102126	0
4	5	0.0036	0.0224	0.0614	0
5	6	0.002975	0.022649	0.066382	0
5	6	0.002975	0.022649	0.066382	0
6	7	0.001695	0.012908	0.03783	0
6	7	0.001695	0.012908	0.03783	0
7	8	0	0.0103	0	0.95
8	9	0.000254	0.0022	0.8792	0
9	10	0	0.01893	0	0.95
10	11	0.00062	0.00339	0.00774	0
10	11	0.00054	2.38	0.00774	0
10	12	0.003	0.00357	0.0416	0
11	12	0.0035	0.0208	0.0568	0
12	13	0.005	0.0289	0.081	0
12	13	0.003152	0.02578	0.0731	0
13	14	0.008403	0.052574	0.08514	0
13	14	0.008106	0.03814	0.0886	0
13	3	0.0079	0.0466	0.1282	0
14	15	0.001485	0.0685	0	0.95
16	5	0.0008	0.0461	0	1.05

A. Controller Design for the Practical Size Power System

The structure of the controller is similar to that in Fig. 6. However, we should notice that the system structure is now totally different with the revised four-machine two-area system in Section IV. Since there is no STATCOM near Zhangdong wind farm to provide reactive power control, thus the only controllable unit is the DFIG itself. Moreover, the system is quite large and robust that it may not demonstrate interarea oscillation after the fault. So the input signal of the controller is redesigned as follows:

$$\begin{cases} \Delta V_{B15}(t)\ \Delta V_{B15}(t-1)\ \Delta V_{B15}(t-2) \\ \Delta P_{B15}(t)\ \Delta P_{B15}(t-1)\ \Delta P_{B15}(t-2) \end{cases} \tag{10}$$

where ΔV_{B15} and ΔP_{B15} are the voltage and active power deviations of Zhangdong wind farm at Bus15, respectively. The output signal of the controller is $\Delta Q_{\text{ref}}(t)$, which acts as

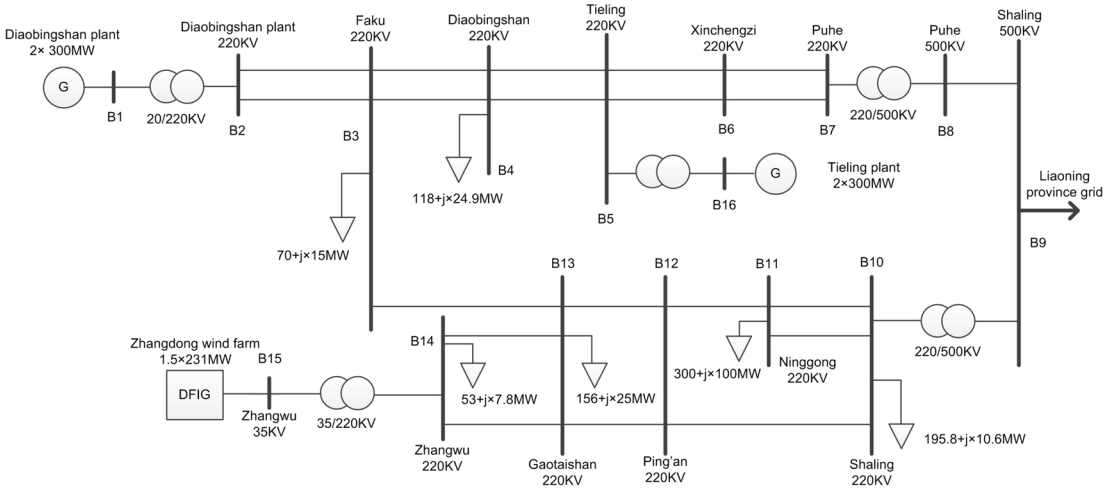

Fig. 13. Schematic diagram of the Liaoning Zhangdong wind farm system.

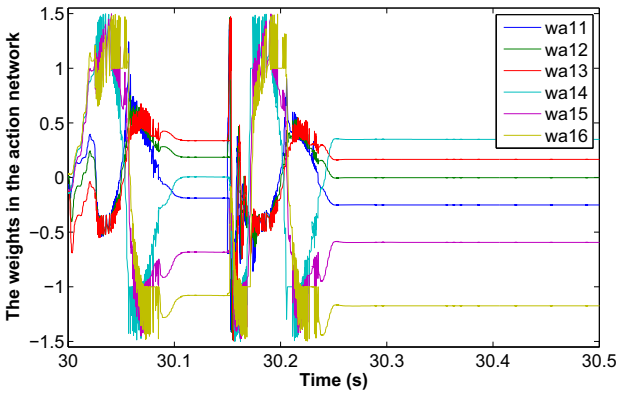

Fig. 14. Learning process has been represented by the evolution of the individual weight connecting the input units to one of the hidden units in the action network.

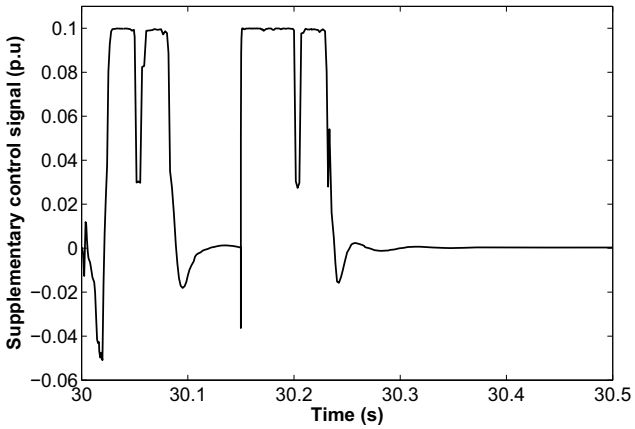

Fig. 15. Supplementary control signal generated by the action network.

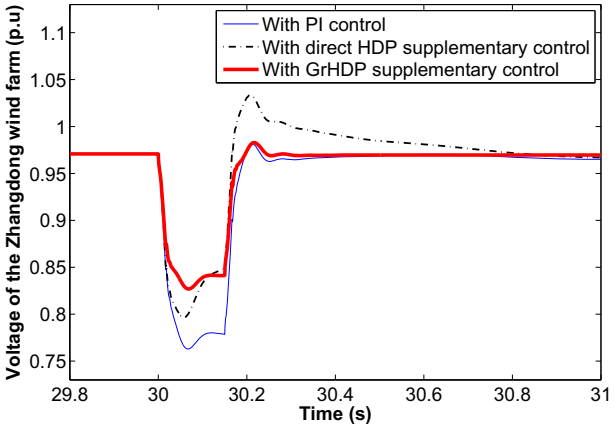

Fig. 16. Performance of Zhangdong wind farm voltage after training.

supplementary reactive power control signal to the wind farm. The reinforcement signal of the controller is redesigned as follows:

$$r(t) = -(\Delta V_{B15}^2(t) + 0.5 * \Delta V_{B15}^2(t-1) + 0.1 * \Delta V_{B15}^2(t-2)) - (\Delta P_{B15}^2(t) + 0.5 * \Delta P_{B15}^2(t-1) + 0.1 * \Delta P_{B15}^2(t-2)). \quad (11)$$

B. Control Results Analysis

A single-phase ground-fault is applied near Ping'an 220 kV bus at 30.0 s. The fault lasted for 150 ms with tripping one of the transmission lines between Gaotaishan and Ping'an. The evolution of the individual weight connecting the input units to one of the hidden units in the action network represents the learning process of the GrHDP controller, and is shown in Fig. 14. We can directly observe that all the weights are converged after 30.3 s. Notice that the fault time (30.0–30.15 s) and post-fault time (30.15–30.3 s) are two different stages to the controller. These two stages fault time alongside the two learning processes are demonstrated in the weights evolution. In each stage, the weights are changing dramatically at the beginning and converged after the adapting occurs. This learning process is consistent with the output supplementary control signal curve as shown in Fig. 15.

After finishing the learning process, the voltage and current of Zhangdong wind farm at Bus15 are improved by the proposed GrHDP controller, compared with the performance

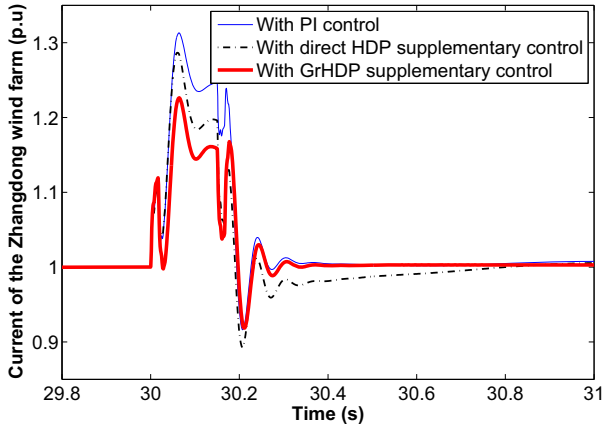

Fig. 17. Performance of Zhangdong wind farm current after training.

of PI controller and direct HDP controller, as shown in Figs. 16 and 17.

VI. Conclusion

In this paper, an adaptive controller based on GrHDP for DFIG-based wind farm is proposed. We presented the detailed control architecture, and also tested the approach on two cases, i.e., a revised four-machine two-area system with wind penetration and a practical size power system with wind farm. Comparative studies of our method with existing approaches were also presented in this paper. Simulation results demonstrated that with the proposed GrHDP controller, the transient stability of the wind farm under grid fault conditions can be improved. LVRT capability of the wind farm and the system could also be enhanced.

The characteristics of the online GrHDP approach is similar to other ADP approaches [21], [22], where the approximation of J is not based on the pretraining data set but on the error functions from interaction with the environment (power plant in this paper) in each time step. However, the formulated temporal difference (TD) learning algorithm in the three networks in GrHDP guaranteed that the expected values of the prediction converge to the correct values, give appropriate samples, and learning iterations [36]. The Robbins–Monro algorithm is the main tool to prove the convergency of the GrHDP approach [37]. A more detailed introduction of the convergency analysis of GrHDP could be referenced in [38].

The adjustment of the weights in the action, critic, and reference network is based on back-propagation that is time-consuming. In real power system applications, the sampling time should be long enough to guarantee the GrHDP controller has adapted the weights in the three networks. During our simulation, it takes about 0.1 ms to fully adapt the weights in the three networks (the iteration number in the reference, action and critic network are set as $N_r = 100$, $N_a = 150$, and $N_c = 120$, respectively) on an Inter(R) Xeon(R) CPU with 3.2 GHz in MATLAB $R2011b$ environment. So the sampling time could be chosen as 2.0 ms (500 Hz) in real power system applications. We should also notice that the reinforcement signal $r(t)$ in (9) requires real-time system signals, therefore the transmission delays in large power systems may impact the controller performance. However, it has been shown that the neural network based control can successfully compensate for the communication delays [39], [40].

There are several interesting directions for future research along this topic. For instance, the supplementary control ability of GrHDP for high-voltage direct current and various FACTS devices could be developed to construct wide-area damping control systems. Since the GrHDP demonstrates robust learning and universal control characteristics, it could also be utilized for stability enhancement of large scale interconnected power systems.

TABLE III
STATCOM Parameters in the Simulation [29]

Parameters	Scenario I	Scenario II
DC Link voltage (kV)	12	40
Total capacitance (μF)	3333	20000
Converter rating (MVA)	10	200

Appendix
STATCOM Parameters

The parameters of the STATCOM used in the first case are shown in Table III.

References

[1] A. Grauers, "Efficiency of three wind energy generator system," *IEEE Trans. Energy Convers.*, vol. 11, no. 3, pp. 650–657, Sep. 1996.
[2] R. Pena, J. C. Clear, and G. M. Asher, "Doubly fed induction generator using back-to-back PWM converters and its application to variable-speed wind energy generation," *IEE Proc. Elect. Power Appl.*, vol. 143, no. 3, pp. 231–241, May 1996.
[3] E. Vittal, M. O'Malley, and A. Keane, "Rotor angle stability with high penetrations of wind generation," *IEEE Trans. Power Syst.*, vol. 27, no. 1, pp. 353–362, Feb. 2012.
[4] L. Yang, Z. Xu, J. Ostergaard, Z. Y. Dong, and K. P. Wong, "Advanced control strategy of DFIG wind turbines for power system fault ride through," *IEEE Trans. Power Syst.*, vol. 27, no. 2, pp. 713–722, May 2012.
[5] A. D. Hansen, P. Sørensen, F. Iov, and F. Blaabjerg, "Control of variable speed wind turbines with doubly-fed induction generators," *Wind Eng.*, vol. 28, no. 4, pp. 411–434, 2004.
[6] N. G. Hingorani and L. Gyugyi, *Understanding FACTS: Concepts and Technology of Flexible AC Transmission Systems.* Hoboken, NJ USA: Wiley, 2000.
[7] M. S. El Moursi, B. Bak-Jensen, and M. H. Abdel-Rahman, "Coordinated voltage control scheme for SEIG-based wind park utilizing substation STATCOM and ULTC transformer," *IEEE Trans. Sustain. Energy*, vol. 2, no. 3, pp. 246–255, Jul. 2011.
[8] C. Han *et al.*, "STATCOM impact study on the integration of a large wind farm into a weak loop power system," *IEEE Trans. Energy Convers.*, vol. 23, no. 1, pp. 226–233, Mar. 2008.
[9] M. Yamamoto and O. Motoyoshi, "Active and reactive power control for doubly-fed wound rotor induction generator," *IEEE Trans. Power Electron.*, vol. 6, no. 4, pp. 624–629, Oct. 1991.
[10] F. Wu, X. P. Zhang, P. Ju, and M. J. H. Sterling, "Decentralized nonlinear control of wind turbine with doubly fed induction generator," *IEEE Trans. Power Syst.*, vol. 23, no. 2, pp. 613–621, May 2008.
[11] F. Wu, X. P. Zhang, K. Godferey, and P. Ju, "Small signal stability analysis and optimal control of a wind turbine with doubly fed induction generator," *IET Gen. Transmiss. Distrib.*, vol. 1, no. 5, pp. 751–760, Sep. 2007.
[12] Y. Tang, P. Ju, H. He, C. Qin, and F. Wu, "Optimized control of DFIG-based wind generation using sensitivity analysis and particle swarm optimization," *IEEE Trans. Smart Grid*, vol. 4, no. 1, pp. 509–520, Mar. 2013.
[13] H. M. Jabr, D. Lu, and N. C. Kar, "Design and implementation of neuro-fuzzy vector control for wind-driven doubly-fed induction generator," *IEEE Trans. Sustain. Energy*, vol. 2, no. 4, pp. 404–413, Oct. 2011.

[14] A. Kusiak and Z. J. Zhang, "Adaptive control of a wind turbine with data mining and swarm intelligence," *IEEE Trans. Sustain. Energy*, vol. 2, no. 1, pp. 28–36, Jan. 2011.

[15] V. Galdi, A. Piccolo, and P. Siano, "Designing an adaptive fuzzy controller for maximum wind energy extraction," *IEEE Trans. Energy Convers.*, vol. 23, no. 2, pp. 559–569, Jun. 2008.

[16] P. J. Werbos, "Computational intelligence for the smart grid-history, challenges, and opportunities," *IEEE Comput. Intell. Mag.*, vol. 6, no. 3, pp. 14–21, Aug. 2011.

[17] G. K. Venayagamoorthy, "Dynamic, stochastic, computational, and scalable technologies for smart grids," *IEEE Comput. Intell. Mag.*, vol. 6, no. 3, pp. 22–35, Aug. 2011.

[18] W. Qiao, R. G. Harley, and G. K. Venayagamoorthy, "Coordinated reactive power control of a large wind farm and a STATCOM using heuristic dynamic programming," *IEEE Trans. Energy Convers.*, vol. 24, no. 2, pp. 493–503, Jun. 2009.

[19] J. Liang, G. K. Venayagamoorthy, and R. G. Harley, "Wide-area measurement based dynamic stochastic optimal power flow control for smart grids with high variability and uncertainty," *IEEE Trans. Smart Grid*, vol. 3, no. 1, pp. 59–69, Mar. 2012.

[20] D. Molina, G. K. Venayagamoorthy, J. Liang, and R. G. Harley, "Intelligent local area signals based damping of power system oscillations using virtual generators and approximate dynamic programming," *IEEE Trans. Smart Grid*, vol. 4, no. 1, pp. 498–508, Mar. 2013.

[21] J. Si and Y. T. Wang, "Online learning control by association and reinforcement," *IEEE Trans. Neural Netw.*, vol. 12, no. 2, pp. 264–276, Mar. 2001.

[22] C. Lu, J. Si, and X. R. Xie, "Direct heuristic dynamic programming for damping oscillations in a large power system," *IEEE Trans. Syst., Man, Cybern. B, Cybern.*, vol. 38, no. 4, pp. 1008–1013, Aug. 2008.

[23] Y. Tang, H. He, Z. Ni, J. Wen, and X. Sui, "Reactive power control of grid-connected wind farm based on adaptive dynamic programming," *Neurocomputing*, vol. 125, pp. 125–133, Feb. 2014.

[24] Y. Tang, H. He, and J. Wen, "Adaptive control for an HVDC transmission link with FACTS and a wind farm," in *Proc. IEEE PES Innov. Smart Grid Technol. (ISGT)*, Washington, DC, USA, Feb. 2013, pp. 1–6.

[25] Y. Tang, H. He, and J. Wen, "Comparative study between HDP and PSS on DFIG damping control," in *Proc. IEEE Symp. Comput. Intell. Appl. Smart Grid (CIASG)*, Singapore, Apr. 2013, pp. 59–65.

[26] X. Sui, Y. Tang, H. He, and J. Wen, "Energy-storage-based lowfrequency oscillation damping control using particle swarm optimization and heuristic dynamic programming," *IEEE Trans. Power Syst.*, vol. 29, no. 5, pp. 2539–2548, Sep. 2014.

[27] H. He, Z. Ni, and J. Fu, "A three-network architecture for on-line learning and optimization based on adaptive dynamic programming," *Neurocomputing*, vol. 78, no. 1, pp. 3–13, 2012.

[28] Z. Ni, H. He, and J. Wen, "Adaptive learning in tracking control based on the dual critic network design," *IEEE Trans. Neural Netw. Learn. Syst.*, vol. 24, no. 6, pp. 913–928, Jun. 2013.

[29] S. Bozhko, G. Asher, R. Li, J. Clare, and L. Yao, "Large offshore DFIG-based wind farm with line-commutated HVDC connection to the main grid: Engineering studies," *IEEE Trans. Energy Convers.*, vol. 23, no. 1, pp. 119–127, Mar. 2008.

[30] P. Kundur, *Power System Stability and Control.* New York, NY, USA: McGraw-Hill, 1994.

[31] F. M. Hughes, O. Anaya-Lara, N. Jenkins, and G. Strbac, "A power system stabilizer for DFIG-based wind generation," *IEEE Trans. Power Syst.*, vol. 21, no. 4, pp. 763–772, May 2006.

[32] N. Kshatriya, U. D. Annakkage, F. M. Hughes, and A. M. Gole, "Optimized partial eigenstructure assignment-based design of a combined PSS and active damping controller for a DFIG," *IEEE Trans. Power Syst.*, vol. 25, no. 2, pp. 866–876, May 2010.

[33] H. Huang and C. Y. Chung, "Coordinated damping control design for DFIG-based wind generation considering power output variation," *IEEE Trans. Power Syst.*, vol. 27, no. 4, pp. 1916–1925, Nov. 2012.

[34] A. Mendonca and J. A. P. Lopes, "Robust tuning of power system stabilisers to install in wind energy conversion systems," *IET Renew. Power Gener.*, vol. 3, no. 4, pp. 465–475, Dec. 2009.

[35] D. Ernst, M. Glavic, and L. Wehenkel, "Power systems stability control: Reinforcement learning framework," *IEEE Trans. Power Syst.*, vol. 19, no. 1, pp. 427–435, Feb. 2004.

[36] R. Sutton and A. Barto, *Reinforcement Learning: An Introduction.* Cambridge, U.K.: Cambridge Univ. Press, 1998.

[37] H. Robbins and S. Monro, "A stochastic approximation method," *Ann. Math. Statist.*, vol. 10, no. 1, pp. 400–407, 1951.

[38] Z. Ni, H. He, J. Wen, and X. Xu, "Goal representation heuristic dynamic programming on maze navigation," *IEEE Trans. Neural Netw. Learn. Syst.*, vol. 24, no. 12, pp. 2038–2050, Dec. 2013.

[39] W. Qiao, G. K. Venayagamoorthy, and R. G. Harley, "Optimal wide-area monitoring and nonlinear adaptive coordinating neurocontrol of a power system with wind power integration and multiple FACTS devices," *Neural Netw.*, vol. 21, no. 2, pp. 466–475, 2008.

[40] N. R. Chaudhuri, B. Chaudhuri, S. Ray, and R. Majumder, "Wide-area phasor power oscillation damping controller: A new approach to handling time-varying signal latency," *IET Gen. Transmiss. Distrib.*, vol. 4, no. 5, pp. 620–630, May 2010.

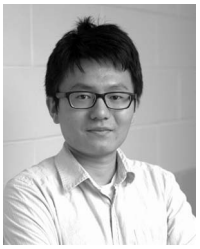

Yufei Tang (S'13) received the B.Eng. and the M.Eng. degrees in electrical engineering from Hohai University, Nanjing, China, in 2008 and 2011, respectively. He is currently pursuing the Ph.D. degree from the Department of Electrical, Computer, and Biomedical Engineering, University of Rhode Island, Kingston, RI, USA.

His current research interests include power system modeling, power system stability control, wind energy generation and integration, smart grids, power system cyber security, and the application of computational intelligence in power systems.

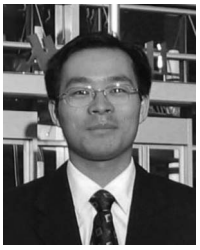

Haibo He (SM'11) received the B.S. and M.S. degrees in electrical engineering from the Huazhong University of Science and Technology, Wuhan, China, in 1999 and 2002, respectively, and the Ph.D. degree in electrical engineering from Ohio University, Athens, USA, in 2006.

From 2006 to 2009, he was an Assistant Professor with the Department of Electrical and Computer Engineering, Stevens Institute of Technology, Hoboken, NJ, USA. He is currently the Robert Haas Endowed Professor of Electrical Engineering with the University of Rhode Island, Kingston, RI, USA. He has published one research book (Wiley), edited one research book (Wiley-IEEE) and six conference proceedings (Springer), and authored and co-authored over 120 peer-reviewed journal and conference papers. His research has been covered by national and international media such as the IEEE Smart Grid Newsletter, *The Wall Street Journal*, and *Providence Business News*. His current research interests include smart grid, cyber security, cyber physical systems, adaptive dynamic programming, machine learning, and computational intelligence and applications.

Prof. He is currently an Associate Editor of the IEEE TRANSACTIONS ON NEURAL NETWORKS AND LEARNING SYSTEMS and the IEEE TRANSACTIONS ON SMART GRID. He was the recipient of the IEEE Computational Intelligence Society Outstanding Early Career Award in 2014, the National Science Foundation CAREER Award in 2011, and the Providence Business News Rising Star Innovator Award in 2011.

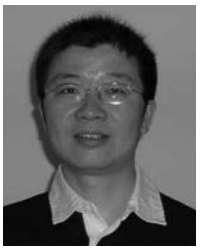

Jinyu Wen (M'10) received the B.Eng. and the Ph.D. degrees in electrical engineering from the Huazhong University of Science and Technology (HUST), Wuhan, China, in 1992 and 1998, respectively.

He was a Visiting Student and a Research Fellow with the University of Liverpool, Liverpool, U.K., from 1996 to 1997 and from 2002 to 2003, respectively, and a Senior Visiting Researcher with the University of Texas at Arlington, Arlington, TX, USA, in 2010. From 1998 to 2002, he was a Director Engineer with XJ Electric Company Ltd., Xuchang, China. In 2003, he joined HUST, Wuhan, China, where he is currently a Professor. His current research interests include renewable energy integration, energy storage application, multiterminal high-voltage direct current, and power system operation and control.

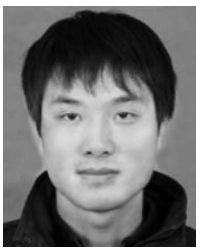

Ju Liu (S'13) received the B.Eng. degree in electrical engineering from the Huazhong University of Science and Technology (HUST), Wuhan, China, in 2011, where he is currently pursuing the Ph.D. degree from the College of Electrical and Electronic Engineering.

His current research interests include large-scale power system operation and control, renewable energy integration, and energy storage applications.